CONTRAST MEDIA & MOLECULAR IMAGING
Contrast Med. Mol. Imaging **1**:246–258 (2006)
Published online 19 October 2006 in Wiley InterScience (www.interscience.wiley.com) DOI:10.1002/cmmi.111

CONTRAST MEDIA & MOLECULAR IMAGING

Full Paper

Targeting of lanthanide(III) chelates of DOTA-type glycoconjugates to the hepatic asyaloglycoprotein receptor: cell internalization and animal imaging studies

*M. I. M. Prata[1], A. C. Santos[1], S. Torres[2], J. P. André[2], J. A. Martins[2], M. Neves[3], M. L. García-Martín[4], T. B. Rodrigues[4,5], P. López-Larrubia[4], S. Cerdán[4] and C. F. G. C. Geraldes[5]**

[1]*Instituto de Biofísica e Biomatemática, Faculdade de Medicina, Universidade de Coimbra, Coimbra, Portugal*
[2]*Centro de Química, Campus de Gualtar, Universidade do Minho, 4710-057 Braga, Portugal*
[3]*Instituto Tecnológico e Nuclear, Sacavém, Portugal*
[4]*Instituto de Investigaciones Biomédicas 'Alberto Sols', CSIC-UAM, Madrid, Spain*
[5]*Departamento de Bioquímica, Centro de RMN e Centro de Neurociências e Biologia Celular, Faculdade de Ciências e Tecnologia, Universidade de Coimbra, Coimbra, Portugal*

Received 10 May 2006; Revised 31 July 2006; Accepted 28 August 2006

ABSTRACT: The characterization of a new class of hydrophilic liver-targeted agents for γ-scintigraphy and MRI, consisting, respectively, of $[^{153}Sm]^{3+}$ or Gd^{3+} complexes of DOTA monoamide or bisamide linked glycoconjugates (DOTA = 1,4,7,10-tetraazacyclododecane-1,4,7,10-tetraacetic acid), is reported. *In vitro* studies show high uptake of radiolabeled $[^{153}Sm]$-$DOTAGal_2$ by the human hepatocyte carcinoma cell line Hep G2 containing the asialoglycoprotein receptor (ASGP-R), which is decreased to less than 50% by the presence of its high-affinity ligand asialofetuin (ASF). *In vivo* biodistribution, γ-imaging and pharmacokinetic studies on Wistar rats using the $[^{153}Sm]^{3+}$-labeled glycoconjugates show a high uptake in the receptor-rich organ liver of the radiolabeled compounds containing terminal galactosyl groups, but very little uptake for those compounds with terminal glycosyl groups. Blocking the receptor *in vivo* reduced liver uptake by 90%, strongly suggesting that the liver uptake of these compounds is mediated by their binding to the asyaloglycoprotein receptor (ASGP-R). This study also demonstrated that the valency increase improves the targeting capability of the glycoconjugates, which is also affected by their topology. However despite the specific liver uptake of the radiolabeled galactose-bearing multivalent compounds, the animal MRI assessment of the corresponding Gd^{3+} chelates shows liver-to-kidney contrast effects which are not significantly better than those shown by GdDTPA. This probably results from the quick wash-out from the liver of these highly hydrophilic complexes, before they can be sufficiently concentrated within the hepatocytes via receptor-mediated endocytosis. Copyright © 2006 John Wiley & Sons, Ltd.

KEYWORDS: magnetic resonance imaging; contrast agents; gadolinium; glycoconjugates; liver targeting; asialoglycoprotein receptor; γ scintigraphy

INTRODUCTION

In humans and animals, oligosacharides are covalently bound to proteins (glycoproteins) and lipids (glycolipids) and control a wide variety of cellular processes. These functions are mediated by a class of membrane receptor proteins belonging to the general family of lectins. Lectins are monomeric or (homo/hetero)-oligomeric proteins, either soluble or membrane-bound, bearing a single or multiple carbohydrate recognizing domain(s)

**Correspondence to*: C. F. G. C. Geraldes, Departamento de Bioquímica, Faculdade de Ciências e Tecnologia, Universidade de Coimbra, Apartado 3126, 3001-401 Coimbra, Portugal. E-mail: geraldes@ci.uc.pt
Contract/grant sponsor: FEDER.
Contract/grant sponsor: III Instituto de Investigação Interdisciplinar University of Coimbra, Portugal; *contract/grant number:* III/BIO/45/2005.
Contract/grant sponsor: Foundation of Science and Technology, Portugal; *contract/grant number:* POCTI/QUI/47005/2002.
Contract/grant sponsor: Institute of Health Carlos III, Spain; *contract/grant number:* PIO051845.

Abbreviations used: AG, arabinogalactan; ASF, asialofetuin; ASGP-R, asialoglycoprotein receptor; BW, body weight; CA, contrast agent; DCE, dynamic contrast enhanced; DTPA, diethylene triamine pentaacetic acid, a linear ligand; DOTA, 1,4,7,10-tetraazacyclododecane-1,4,7,10-tetraacetic acid, a macrocyclic ligand; DOTAGal, $DOTAGal_2$, $DOTAGal_4$, are DOTA monoamide derivatives with one, two and four terminal galactosyl groups; DOTALac and $DOTALac_2$, the same with one and two terminal lactosyl groups; DOTAGlc and $DOTAGlc_2$, the same with one and two terminal glycosyl groups; $DO2AGal_2$, DOTA *cis*-bisamide derivative with one terminal galactosyl group at each amide substituent; FBS, fetal bovine serum; FOV, field of view; GSA, galactosylated serum albumin; ID, injected dose; MEM, minimum essential medium; MION, monocrystalline iron oxide nanoparticles; PBS, modified phosphate-buffered saline; PL, polylysine; RARE, rapid acquisition and relaxation enhancement, fast spin echo MRI method; SPECT, single photon emission computed tomography; T_1, spin-lattice relaxation time in MR; *TE*, echo time; *TR*, repetition time; USPIO, ultra-small superparamagnetic iron oxide particles.

(CRD) per subunit (1,2). The CRDs interact specifically with sugars (glucose, mannose, galactose, etc) with affinity constants (lectin-monomeric sugar) (K_d) in the milimolar range (3). Assembly of monomeric units produces oligomeric lectins displaying an array of CRDs with a variety of topologies (4). Often one or both of the interacting sugar–lectin partners are membrane-bound. A membrane-bound lectin (receptor) may recognize a soluble or a membrane-bound oligosaccharide (5). Both types of interactions are appealing for pharmacologic intervention as long as the intrinsically low monomeric sugar–lectin affinity can be overcome (6). The use of soluble multivalent glycoconjugate constructs displaying a *cluster glycosid effect* is mandatory for the targeting of cell/organ-specific lectins for drug delivery purposes and for the inhibition of cell–cell or cell–foreign body (bacteria/virus) interactions (7,8). The hepatic asialoglycoprotein receptor (ASGP-R) is an organ-specific lectin, not found anywhere else in the body except on the surface of hepatocytes. This hetero-oligomeric lectin has affinity for terminal β-galactoside and β-*N*-acetyl-galactosaminyl residues on glycoproteins. Although its precise function *in vivo* is still unclear, it is involved in selectively removing de-sialylated glycoproteins, with exposed terminal galactose residues, from serum (9). In addition to asialoglycoproteins, the ASGP-R recognizes β-galactoside and *N*-acetyl-β-galactosaminyl residues appended to a variety of artificial molecular scaffolds (10–13).

Annually many people die worldwide of liver cancer following hepatitis B. The functional imaging of liver ASGP-R is of both diagnostic and prognostic value during treatment of liver cancer and other liver conditions (14–16). Molecular constructs bearing efficient reporter groups and pendant β-galactoside and/or *N*-acetyl-β-galactosaminyl residues can lead to hepatocyte-specific imaging agents for liver (11,14–16). A conjugate of a neoglycoprotein, galactosylated serum albumin (GSA), with [^{99m}Tc]-DTPA (diethylene triamine pentaacetic acid), [^{99m}Tc]-DTPA-GSA, has been used in SPECT (single photon emission computed tomography) hepatic imaging to assess the ASGP-R function in mice (17). The hepatocyte-specific nature of the ASGP-R and the fact that it is still expressed (although in reduced numbers) on hepatoma cells makes it possible to detect liver cancer metastases to other organs. The same imaging agent, [^{99m}Tc]-DTPA-GSA, has been demonstrated to be clinically useful in humans to detect liver cancer metastases to the bones (18) and to assess de dynamics of the ASGP-R internalization/recycling to the surface of the hepatocytes (19,20). A GdDTPA conjugate of polylysine (PL) derivatized with galactosyl groups (GdDTPA-gal-PL) (21), as well as a spin-labeled arabinogalactan (22), have also been developed as macromolecular potential contrast agents for liver MRI by targeting the hepatocyte ASGP-R. A variety of particulate systems targeted to the ASGP-R have also been tested in cells and mice as potential contrast agents for liver MRI: monocrystalline iron oxide nanoparticles (MION) conjugated to the bovine plasma protein asialofetuin (ASF), MION-ASF (23), arabinogalactan (AG)-coated ultra-small superparamagnetic iron oxide particles (USPIO), AG-USPIO (24–27). Both the macromolecular and particle-based ASGP-R-targeted imaging agents described above include carriers bearing multiple reporter groups and a multivalent display of galactosyl targeting groups. However these agents are inherently polydisperse and ill characterized. Chemically well-defined and characterized multivalent agents can be assembled by an alternative molecular design: the conjugation of dendrimeric clustered carbohydrate bifunctional reagents (monodisperse, well defined and characterized) to a reporter group (28). The resulting conjugates are of substantially lower molecular weight, higher stability and greater biological safety. Previous to our report on the synthesis of dendrimeric multivalent glycoconjugates of metal complexes for molecular imaging (MRI and scintigraphy) (29–31), only a study describing the use of a low molecular weight, well-characterized, monomeric [^{111}In]-radiolabeled galactopyranosyl conjugate of DOTA (1,4,7,10-tetraazacyclododecane-1,4,7,10-tetraacetic acid) for the targeting of the ASGP-R both in hepatic cell lines and mice had appeared in the literature (32). The design of lectin-targeted MRI imaging agents includes a reporter group, consisting of a chelator binding lanthanide(III) ion with high kinetic and thermodynamic stability, and a targeting group consisting of a clustered carbohydrate of variable valence, containing an increasing number of terminal galactosyl groups and capable of interacting with high affinity and selectivity with endogenous lectins such as the ASGP-R (3,29–31).

Here we report the radiolabeling of a series of glycoconjugates based on DOTA-monoamide and bisamide functionalized chelators (Fig. 1) with [^{153}Sm]$^{3+}$ and their evaluation using i*n vitro* studies in the human hepatocyte carcinoma cell line Hep G2. DOTA-like chelators are well known to form lanthanide(III) chelates of high thermodynamic and kinetic stability, which is of crucial importance for *in vivo* applications (33). Dynamic γ-scintigraphic studies of the pharmacokinetics of the [^{153}Sm]$^{3+}$-labeled glycoconjugates and their biodistribution in Wistar rats are also described, revealing the effect of valence and type of the terminal sugar moiety on their liver targeting efficacy. We also report an *in vivo* MRI study of the contrast effects and pharmacokinetics of the Gd^{3+} complexes of the divalent glycoconjugates $DOTALac_2$ (**2c**), $DOTAGal_2$ (**2a**) and $DOTAGlc_2$ (**2b**) (Fig. 1) in mice, compared with a typical commercial, small molecular weight contrast agent, GdDTPA (Magnevist®).

EXPERIMENTAL

The synthesis of the monovalent DOTAGal, DOTALac and DOTAGlc (**1**), divalent $DOTAGal_2$, $DOTALac_2$ and

DOI: 10.1002/cmmi

DOTAGlc$_2$ (**2**) and tetravalent DOTAGal$_4$ (**4**) monoamide glycoconjugate ligands (29), as well as of the divalent DO2A(*cis*)Gal$_2$ bisamide (**3**) ligand (31), have been described previously.

Reagents for cell interaction, γ-imaging and biodistribution studies

[^{153}Sm]Samarium chloride ([^{153}Sm]Cl$_3$) was produced at the ITN (Instituto Tecnológico e Nuclear), Lisbon, with a specific activity >5 GBq/mg. For this purpose, [^{153}Sm] samarium oxide ([^{153}Sm]$_2$O$_3$) was prepared from a 98% [^{152}Sm]-enriched samarium oxide target, sealed into a quartz vial and welded into an aluminium can, by neutron irradiation using a thermal flux of 2.3×10^{13} n/cm^2 s. Following irradiation, the sample was opened, dissolved in 1 M HCl and the final [^{153}Sm]samarium chloride (^{153}SmCl$_3$) was brought to a stock concentration of 1.9×10^{-3} M.

Radiotracer preparation

Stock solutions of the ligands were prepared in isotonic HEPES buffer (pH 7) or sodium acetate buffer (0.4 M,

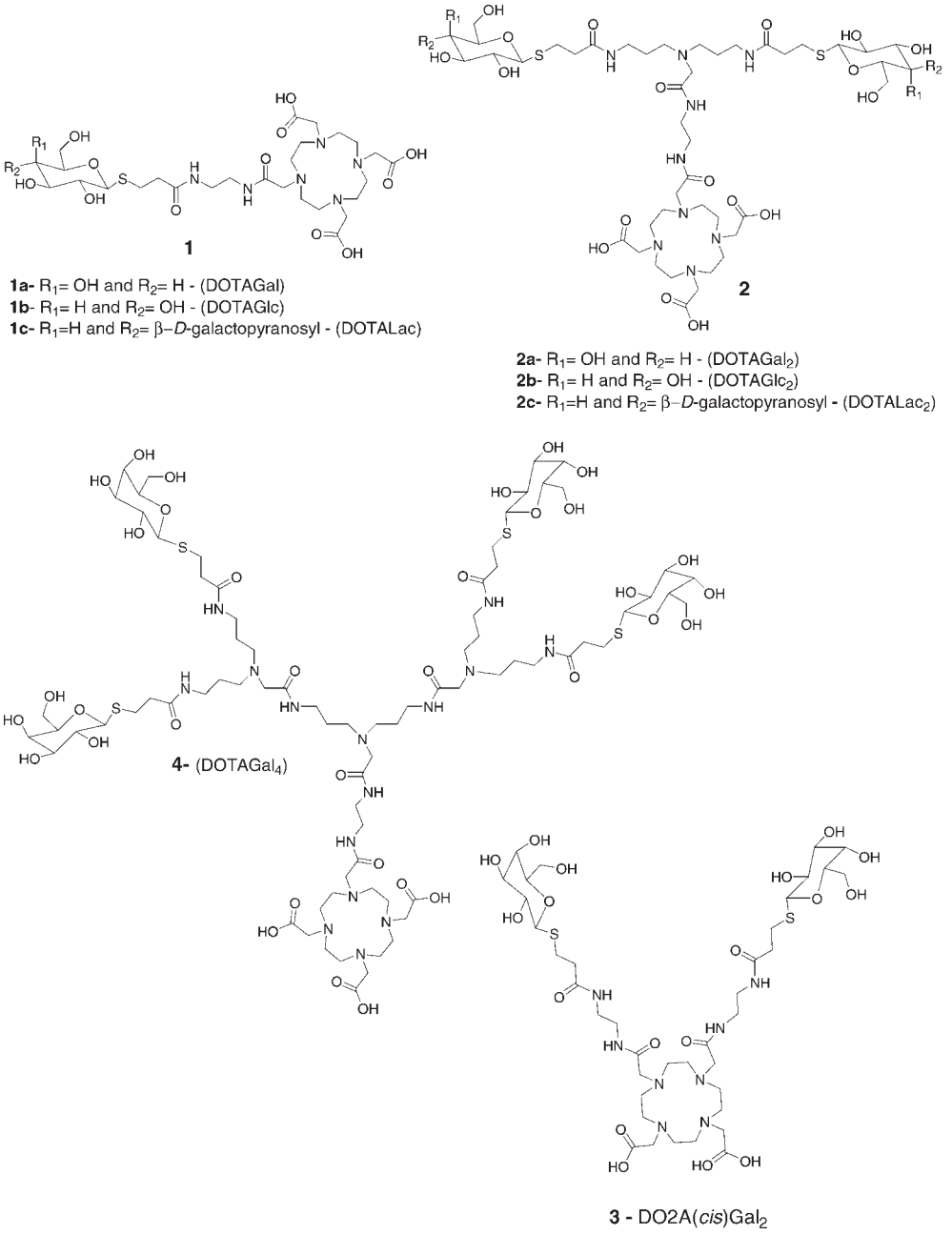

Figure 1. Structure of monovalent (**1**), divalent (**2** and **3**) and tetravalent (**4**) glycoconjugate ligands.

DOI: 10.1002/cmmi

pH 5); and mixed with [^{153}Sm]samarium chloride and the solution was heated at 60°C for 3 h. A quality control was performed by thin-layer chromatography (TLC), using water:ethanol:dicloromethane:ammonia, 5:5:5:1, as eluent.

Serum stability

To 3 ml of fresh human serum previously equilibrated in a 5% CO_2 (95% air) environment at 37°C, was added 5 μCi of the [^{153}Sm]-DOTAGal standard solution. The mixture was stored in a 37°C environment. At appropriate periods of time (0, 30 min, 1 and 4 h) 100 μL aliquots (in triplicate) were removed and treated with 200 μL of ethanol. Samples were then cooled (4°C) and centrifuged for 15 min, at 4000 rpm and 4°C, to precipitate serum proteins. A 100 μL aliquot of supernatant was removed for activity counting in a γ well-counter. The sediment was washed twice with 1 ml of ethanol and counted. The activities in the supernatant and in the pellet were compared as (activity in the pellet/activity in supernatant) × 100.

In vitro cell interaction studies

Hep G2 human hepatoma cell line (ECACC, UK) was grown in 75 ml bottles with MEM (minimum essential medium) from Sigma, supplemented with 10% FBS (fetal bovine serum) from Gibco Invitrogen, and non-essential aminoacids, glutamine and penicillin/streptomycin, all from Sigma. The cells were counted and transferred to a six-hole multiwell plate (0.2 million cells/hole), 2 ml of medium were added to each hole and then the cells were incubated at 37°C, under 5% CO_2 for the period necessary to obtain cell confluence. This is needed because the human hepatocyte carcinoma line Hep G2 expresses maximum receptor activity only in confluent cultures (34). The medium was changed every day. On the day of the experiments the medium was removed and the cells were washed twice with 1.5 ml medium before adding 1.2 ml medium and they were allowed to adjust for 1 h at 37°C. Approximately 1 μCi of radioligand was added in each well to the medium and the cells were incubated for 30 min and 1 and 2 h at 37°C. To three of the holes in each plate was added an excess of asialofetuin (Sigma; 200 μl of a 0.2 mg/ml solution) (32) to evaluate the contribution of nonspecific contributions to the cell uptake of the glycoconjugates. At appropriate time periods the experiment was stopped by removal of the medium and washing the cells twice with 750 μl ice-cold phosphate buffered saline. The medium plus PBS was collected to tubes to measure the radioactivity. Finally, the cells were treated with 1 M NaOH (1 ml) and incubated at 37°C for 10 min, to detach them from the plates, and the radioactivity was measured in a γ-counter. Each experiment was carried out simultaneously in triplicate.

In vivo γ-imaging

A γ camera-computer system (GE 400 GenieAcq, from General Electric, Milwaukee, WI, USA) was used for acquisition and pre-processing. Data processing and display were performed on a personal computer using homemade software developed for the IDL 5.2 computer tool. A well counter (DPC-Gamma C_{12}, LA, USA) with a Compaq DeskPro compatible computer was used for activity counting in the biodistribution studies.

Gamma images and biological distribution for the [^{153}Sm]$^{3+}$complexes were determined using (200–250 g) Wistar rats. All animal studies were carried out in compliance with procedures approved by the appropriate institutional review committees. Conscious rats were allowed free access to food and water. Groups of four animals (one group for each complex) were anesthetized with ketamine (50 mg/ml)–chloropromazine (2.5%) (10:3) and injected in the femoral vein with ca. 400 μCi of the respective [^{153}Sm]$^{3+}$chelate. The animals were then positioned in dorsal *decubitus* over the detector. Image acquisition was initiated immediately after radiotracer injection. Sequences of 180 images (of 10 s each), were acquired to 64 × 64 matrices. In addition, static data were acquired 24 h after the radiotracer injection.

Images were subsequently processed using an IDL based program (Interactive Data Language, Research Systems, Boulder, CO, USA). In order to analyze the transport of radiotracer over time, three regions of interest (ROI) were drawn on the image files, corresponding to the thorax, liver and left kidney. From these regions, time–activity curves were obtained.

Biodistribution studies

Groups of four animals were injected in the tail vein with ca. 100 μCi of the respective [^{153}Sm]$^{3+}$ tracer and sacrificed 1 h later. The major organs were excised, weighed and tissue radioactivity measured in a γ well-counter. Similar biodistribution studies were also performed with the animals referred to in the previous section sacrificed at 24 h. For determination of non-specific uptake on receptor-positive organs, a group of four animals was co-injected in the femoral vein with a solution of asialofetuin in NaCl (2 mg/ml; injected volume, 200 μl, 0.2 mg asialofetuin/100 g body weight) and [^{153}Sm]$^{3+}$–DOTAGal$_2$ (200 μl).

Magnetic resonance imaging

The MRI experiments were performed on a Bruker Pharmascan system (Bruker Medical Gmbh, Ettlingen,

DOI: 10.1002/cmmi

Germany) using a 7.0 T horizontal-bore superconducting magnet, equipped with a ^{1}H selective birdcage resonator of 38 mm and a Bruker gradient insert with 90 mm diameter (maximum intensity 300 mT/m). All the data were acquired using a Hewlett-Packard console running Paravision software (Bruker Medical Gmbh, Ettlingen, Germany) operating on a Linux platform. Anesthesia was initiated by inhalation in an induction box with O_2 (1 l/min) containing 3% isofluorane, and maintained during the experiment using a mask and 1–2% isofluorane in O_2. Animals, albine Swiss male mice, weighing 19–26 g, were taped down gently into a holder, to minimize breathing-related motion, and were then placed in a heated probe, which maintained the core body temperature at approximately 37°C, monitored by a rectal probe. The physiological state of the animal was monitored by a Biotrig physiological monitor (Bruker Medical Gmbh, Ettlingen, Germany) using the respiratory rate and body temperature. The contrast agents were injected as a bolus of 50 μl via a tail vein catheter at a dose of 0.3 mmol Gd kg^{-1} body weight (BW), except for GdDTPA (Magnevist®, Schering AG, Berlin, Germany), where a dose of 0.2 mmol Gd kg^{-1} BW was used.

For anatomical reference, a multi-slice rapid acquisition and relaxation enhancement (RARE) sequence (35) was performed with the following parameters: RARE factor = 8, $TR = 4000$ ms, effective $TE = 65$ ms, averages = 2, six coronal slices, slice thickness 1.2 mm, FOV = 3.8 cm, matrix = 256 × 256. Then, regional contrast agent uptake was assessed. A series of T_1-weighted spin echo images was sequentially acquired over 1 h following the injection of the contrast agent. The acquisition parameters were: $TR = 155$ ms, $TE = 11.76$ ms, averages = 2, six coronal slices, slice thickness 1.2 mm, FOV = 3.8 cm, matrix = 256 × 256, 60 repetitions with temporal resolution 59.31 s.

MRI data processing

Data were analyzed with software written in-house in IDL. With the aim of comparing the pharmacokinetics obtained from different animals, the data were normalized by calculating the relative, rather than the absolute, enhancement (RE):

$$\mathrm{RE} = \frac{(I - I_0)}{I_0} \times 100$$

where I is the signal intensity at any given time after contrast agent (CA) injection and I_0 is the intensity before injection.

Pharmacokinetics were analyzed by calculating the average enhancements within four different ROIs placed on the liver, kidney medulla, kidney cortex and muscle.

RESULTS AND DISCUSSION

Studies of $[^{153}Sm]^{3+}$-radiolabeled glycoconjugates

Quality control analysis. All the radioactive complexes where analysed by TLC for radiochemical purity determination as described in the Experimental section. The radiochemical purity was >98% for all the $[^{153}Sm^{3+}]$ complexes with a specific activity *ca* 2 mCi/μmol.

Stability in serum. The percentage of radioactivity in the non-proteic fraction of human serum incubated with

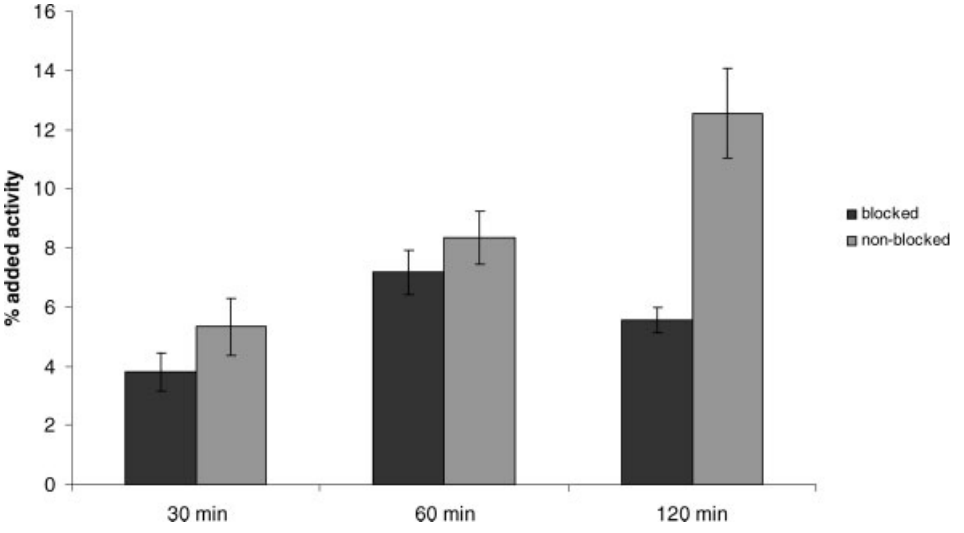

Figure 2. Uptake of $[^{153}Sm]^{3+}$–$DOTAGal_2$, stated as a percentage of added activity, by 1 million Hep G2 cells incubated at different times at 37°C, 5% CO_2 with the radioligand (non-blocked experiments) and effect of the addition of an excess of asialofetuin to the cells (blocked experiment).

DOI: 10.1002/cmmi

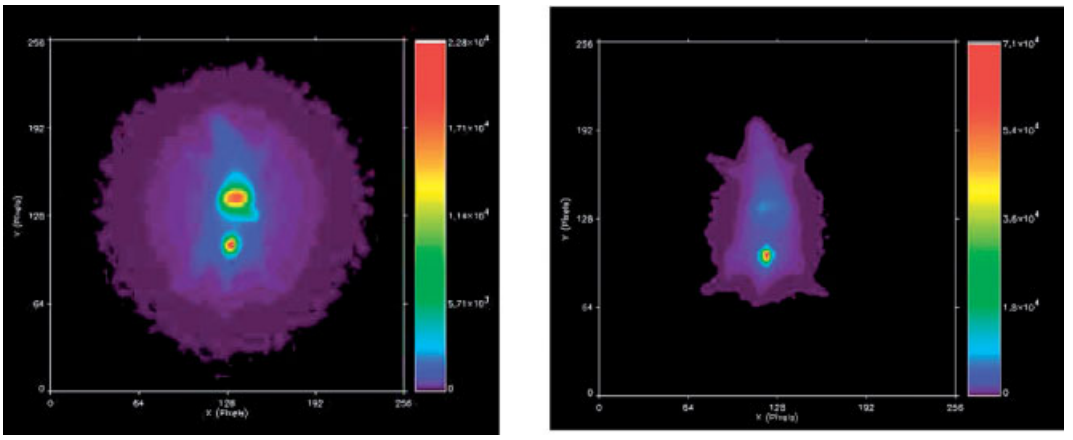

Figure 3. Scintigraphic images of Wistar rats at 30 min after injection with (from left to right) $[^{153}Sm]^{3+}$–$DOTAGal_2$ and $[^{153}Sm]^{3+}$–$DOTAGlc_2$.

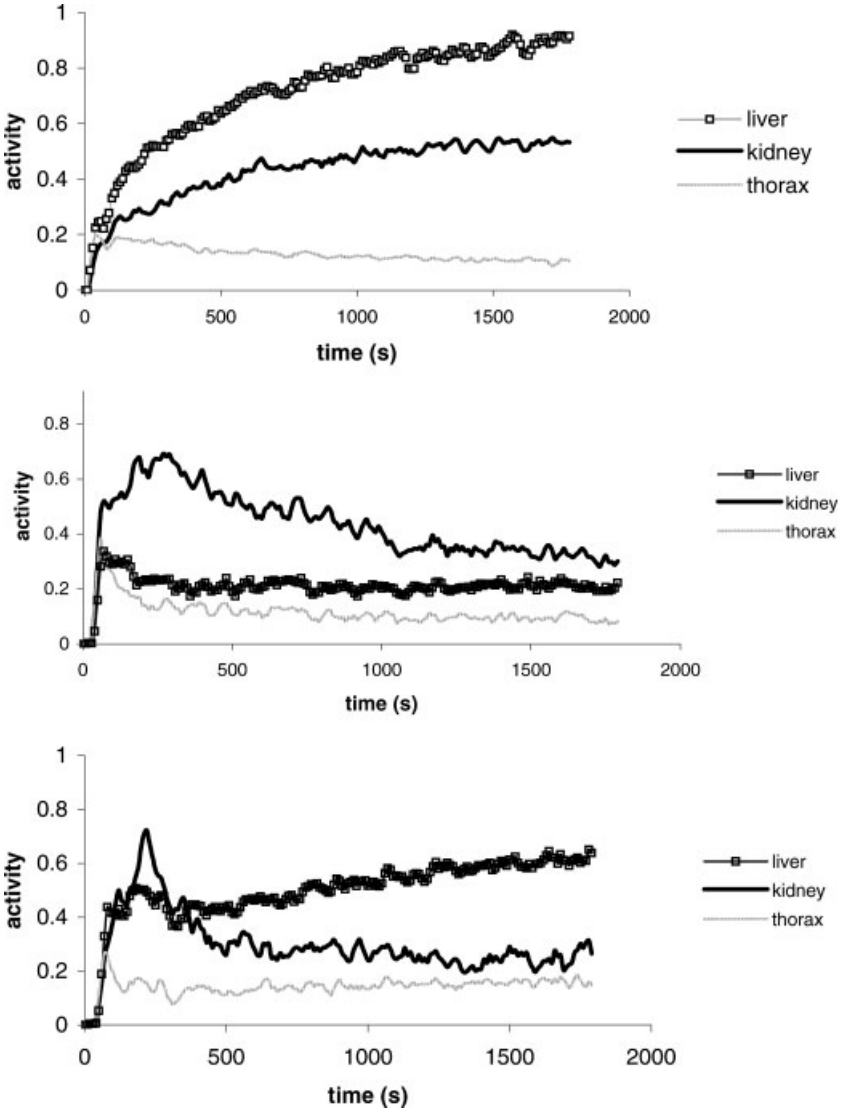

Figure 4. Time–activity curves at the various ROIs in Wistar rats for: from bottom to top $[^{153}Sm]^{3+}$–$DOTALac_2$, $[^{153}Sm]^{3+}$–$DOTAGlc_2$ and $[^{153}Sm]^{3+}$–$DOTAGal_2$.

DOI: 10.1002/cmmi

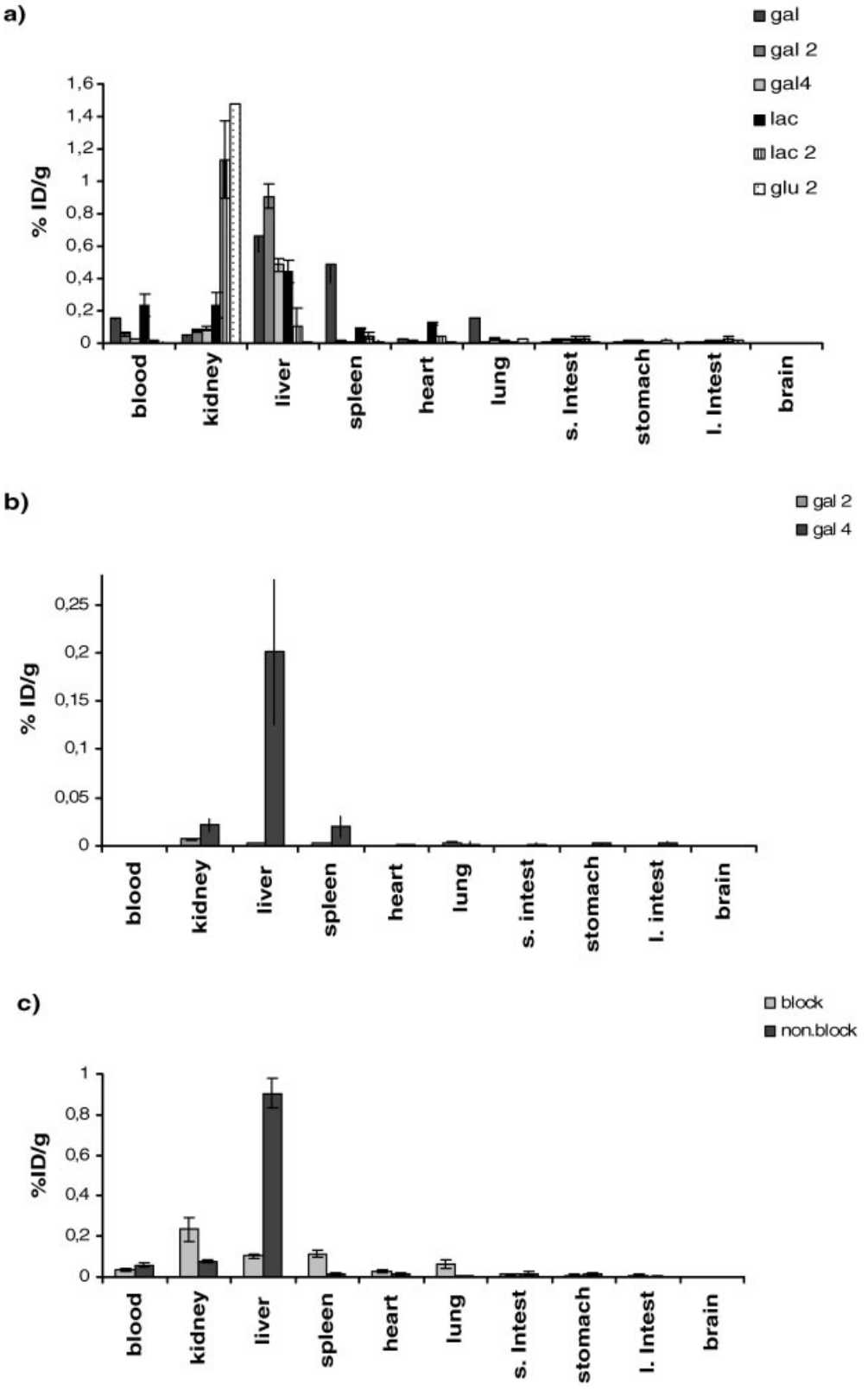

Figure 5. Biodistribution in Wistar rats: (a) $[^{153}Sm]^{3+}$–DOTA glycoconjugates at 1 h post-injection; (b) $[^{153}Sm]^{3+}$–DOTA glycoconjugates at 24 h post-injection; (c) 1 h after i.v. co-injection of $[^{153}Sm]^{3+}$–$DOTAGal_2$ and excess of asialofetuin (block) or without excess of asialofetuin (non-block); results are the means of groups of four animals.

DOI: 10.1002/cmmi

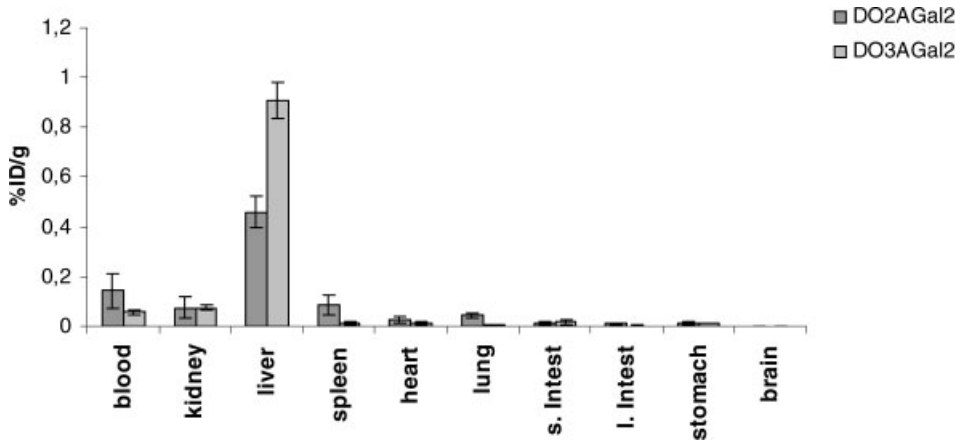

Figure 6. Comparison of the biodistribution in Wistar rates 1 h after injection of $[^{153}Sm]^{3+}$–DO3AGal$_2$ and $[^{153}Sm]^{3+}$–DO2AGlc$_2$.

5 μCi of the $[^{153}Sm]^{3+}$-labeled chelates slowly decays as a function of time (data not shown). For example, in the case of $[^{153}Sm]^{3+}$–DOTAGal *ca* 90% of the activity remained in the non-proteic fraction after 4 h.

Cell uptake. The Hep G2 human hepatocyte carcinoma cell line is known to express ASGP-R both *in vivo* and *in vitro* (34,36). Figure 2 shows the time dependence of the radioligand $[^{153}Sm]^{3+}$–DOTAGal$_2$ uptake in Hep G2 at 37°C with and without ASGP-R blocking. In these conditions, unblocked cell uptake increases with time, reaching 12.6% of the added activity after 2 h, but without reaching a plateau within the 2 h incubation. The cell activity uptake is reduced in the presence of an excess of the ASGP-R blocker asialofetuin (Fig. 2). However, the observed reduction of the radioligand uptake in the presence of excess asialofetuin is smaller than expected if the radioligand bound exclusively to the ASGP-R, especially at short incubation times. This indicates significant nonspecific cell internalization through an unknown mechanism. The specific/nonspecific internalization ratio reaches a maximum at 2 h, when the cell uptake becomes less than 40% of the non-blocked value (the two tailed *t*-test for the 2 h results gives $p = 0.002$ while for 30 min and for 1 h $p > 0.04$), in agreement with similar uptake studies with an $[^{111}In]^{3+}$-labeled DOTA-Gal monoamide (32).

***In vivo* γ-imaging and biodistribution.** Figure 3 shows scintigraphic images of Wistar rats obtained 30 min after tracer injection for $[^{153}Sm]^{3+}$-labeled DOTAGal$_2$ (**2a**) and DOTAGlc$_2$ (**2b**) conjugates. There is a noticeably high uptake of $[^{153}Sm]^{3+}$–DOTAGal$_2$ by liver (left image), correlating with the fact that the surface of liver parenchimal cells contain a very high density of ASGP-R, about 500,000 per cell (37,38), which can selectively take up the radiotracer by receptor mediated endocytosis (32). In the left image the bladder is also seen, which reflects the renal excretion pathway of these hydrophilic compounds. In addition, a very rapid clearance occurs from all other organs, in accordance with the biodistribution data obtained in the same animals (see below). A quite different behavior is found in rats injected with $[^{153}Sm]^{3+}$–DOTAGlc$_2$ (right image), as the activity is localized only in the kidneys. No liver uptake is observed, which is consistent with the fact that glucosyl glycoconjugates are not recognized by the ASGP-Rs (39). The time–activity curves for the $[^{153}Sm]^{3+}$-labeled glycoconjugates were obtained from the dynamic acquisition experiments (Fig. 4). The curves were smoothed and normalized in relation to the maximum activity obtained for each radiolabeled glycoconjugate. While the activity of $[^{153}Sm]^{3+}$–DOTAGal$_2$ is higher in the liver than in the kidney, and steadily increases up to the 30 min time interval in both organs, the activity of $[^{153}Sm]^{3+}$–DOTAGlc$_2$ quickly rises in kidney to a much higher value than in liver, reaching a maximum at 5 min, and then slowly decays. The initial behavior of $[^{153}Sm]^{3+}$–DOTALac$_2$, with a quick activity increase in kidney, is close to that of $[^{153}Sm]^{3+}$–DOTAGlc$_2$, but after attaining a maximum at 4 min, the kidney activity quicky decreases, while the liver activity steadily rises, as in $[^{153}Sm]^{3+}$–DOTAGal$_2$. This result might be explained by the higher hydrophilicity of the lactosyl conjugate relative to the galactosyl conjugate, which determines its initial concentration in the kidney, after which the terminal galactosyl groups of the lactosyl derivative bind to the liver ASGP-Rs. A number of lactosyl conjugates have been described for liver targeting (40,41).

Biodistribution data for the $[^{153}Sm]^{3+}$-radiolabeled glycoconjugates obtained in Wistar rats are presented in Figs 5 and 6 and Table 1 as percentages of injected dose per gram of tissue (%ID/g). The most striking feature shown by the biodistribution studies at 1 h post-injection is the high liver targeting ability of the galactosyl conjugates [Fig. 5(a)]. In sharp contrast, the glucosyl

DOI: 10.1002/cmmi

Table 1. Biodistribution of $[^{153}Sm]^{3+}$–DOTA glycoconjugates at 1 and 24 h post-injection in Wistar rats. Results are the mean of groups of four animals

	Glc_2(2b)	Lac_2(2c)	Gal (1a)	Gal_2 (2a)		Gal_4(3)	
Tissue	1 h	1 h	1 h	1 h	24 h	1 h	24 h
Blood	$0.002 \pm 5 \times 10^{-4}$	0.015 ± 0.005	0.158 ± 0.01	$0.057 \pm 9 \times 10^{-4}$	$5 \times 10^{-5} \pm 2 \times 10^{-5}$	$0.028 \pm 8 \times 10^{-4}$	$1 \times 10^{-4} \pm 4 \times 10^{-5}$
Kidney	1.48 ± 0.001	1.13 ± 0.240	0.0540 ± 0.01	0.075 ± 0.009	$0.007 \pm 5 \times 10^{-5}$	0.091 ± 0.015	0.022 ± 0.007
Liver	0.011 ± 0.002	0.106 ± 0.011	0.66 ± 0.09	0.9062 ± 0.073	$0.023 \pm 3 \times 10^{-4}$	0.428 ± 0.035	0.201 ± 0.008
Spleen	0.012 ± 0.003	0.046 ± 0.002	0.49 ± 0.12	0.012 ± 0.006	$0.003 \pm 2 \times 10^{-6}$	0.006 ± 0.0005	0.020 ± 0.001
Heart	0.006 ± 0.0006	$0.047 \pm 2 \times 10^{-4}$	0.026 ± 0.0006	0.0138 ± 0.006	$2 \times 10^{-4} \pm 6 \times 10^{-4}$	0.010 ± 0.0022	$0.002 \pm 4 \times 10^{-4}$
Lung	0.022 ± 0.0002	0.051 ± 0.003	0.1590 ± 0.003	0.008 ± 0.002	$5 \times 10^{-4} \pm 3 \times 10^{-6}$	0.027 ± 0.008	0.002 ± 0.0002
Small inntestine	$0.009 \pm 5 \times 10^{-4}$	0.025 ± 0.016	0.0110 ± 0.005	0.0167 ± 0.0084	$3 \times 10^{-4} \pm 2 \times 10^{-5}$	0.021 ± 0.0021	$0.002 \pm 4 \times 10^{-4}$
Large intestine	0.014 ± 0.0027	0.029 ± 0.017	0.011 ± 0.004	0.0029 ± 0.001	$6 \times 10^{-4} \pm 3 \times 10^{-6}$	0.013 ± 0.0018	$0.003 \pm 6 \times 10^{-4}$
Stomach	0.0190 ± 0.004	0.004 ± 0.002	0.012 ± 0.0001	0.0121 ± 0.005	$4 \times 10^{-4} \pm 2 \times 10^{-5}$	0.014 ± 0.0018	$0.002 \pm 7 \times 10^{-4}$
Brain	$3 \times 10^{-4} \pm 2 \times 10^{-5}$	$2 \times 10^{-4} \pm 9 \times 10^{-5}$	$3 \times 10^{-4} \pm 0.0005$	0.0007 ± 0.0002	$6 \times 10^{-5} \pm 6 \times 10^{-6}$	$4 \times 10^{-4} \pm 1 \times 10^{-4}$	$2 \times 10^{-5} \pm 4 \times 10^{-6}$

conjugates show no liver uptake, as they locate mainly in the kidneys due to their hydrophilicity. The biodistribution data for the lactosyl conjugates confirm the intermediate behavior between the galactosyl and glucosyl conjugates seen in the dynamic acquisition curves described above.

Another noteworthy finding is the effect of the valence of the glycoconjugates on the biodistribution pattern. Whereas the monovalent conjugate $[^{153}Sm]^{3+}$–DOTAGal shows some spleen and lung uptake, the divalent compound, apart from the kidney, does not appear to a significant extent in any other organ. The behavior of the tetravalent compound is very similar to that of the divalent one (e.g. liver uptake corresponds to 0.91% of the ID/g for $[^{153}Sm]$–$DOTAGal_2$ and to 0.82% of the ID/g for $[^{153}Sm]^{3+}$–$DOTAGal_4$), indicating that the effect of the increase in valence from 2 to 4 does not seem to improve liver uptake after 1 h. This might be explained by the high number of ASGP-Rs expressed by each hepatocyte cell (37,38) and/or some degree of steric crowding of the galactose residues. However, the effect of the valence of synthetic and natural glycoconjugates on the affinity to lectins has been fully demonstrated (7,8) and thus the expected order of increasing affinity of the glycoconjugate ligands for the ASGP-R is tetra > tri > di > mono (7,8,42,43). This is confirmed by the observed contrast in the biodistribution behavior between the $[^{153}Sm]^{3+}$–$DOTAGal_2$ and $[^{153}Sm]^{3+}$–$DOTAGal_4$ derivatives after 24 h [Fig. 5(b), Table 1]. The activity remaining in liver at 24 h for the tetravalent radiolabeled glycoconjugate $[^{153}Sm]^{3+}$–$DOTAGal_4$ (0.2% of the ID/g) is much higher than for the divalent $^{153}Sm^{3+}$–$DOTAGal_2$ (0.002% of the ID/g), suggesting a greater metabolic stability of the former compound.

The data in Fig. 5(a) also shows that the three ligands bearing only one sugar moiety (DOTAGal, DOTAGlc and DOTALac) stay longer in the blood stream and have a more dispersed biodistribution pattern than the higher valence analogs. Binding to some plasma component might be responsable for this finding. Thus, in addition to the multivalence effect, subtle structural effects arising from the dendrimeric framework of these ligands, especially the tertiary amine nitrogen, might be responsable for the observed differences of biodistribution between the monovalent and multivalent compounds.

Figure 5(c) shows the biodistribution results of an *in vivo* competition experiment using large excess of asialofetuin, a specific blocker of the ASGP-R, co-injected with the radioligand $[^{153}Sm]^{3+}$–$DOTAGal_2$. In animals injected with the blocker, activity uptake in liver was reduced by 90% ($p < 0.001$) compared with the blocked animals (32). The injection of the blocking dose also increased the uptake in the kidneys by a factor of 3, suggesting that more activity is cleared instead of binding to the ASGP-R. These results strongly suggest that the uptake of the radiolabeled glycoconjugate is specific to the ASGP-R endocytosis. These results are in close

DOI: 10.1002/cmmi

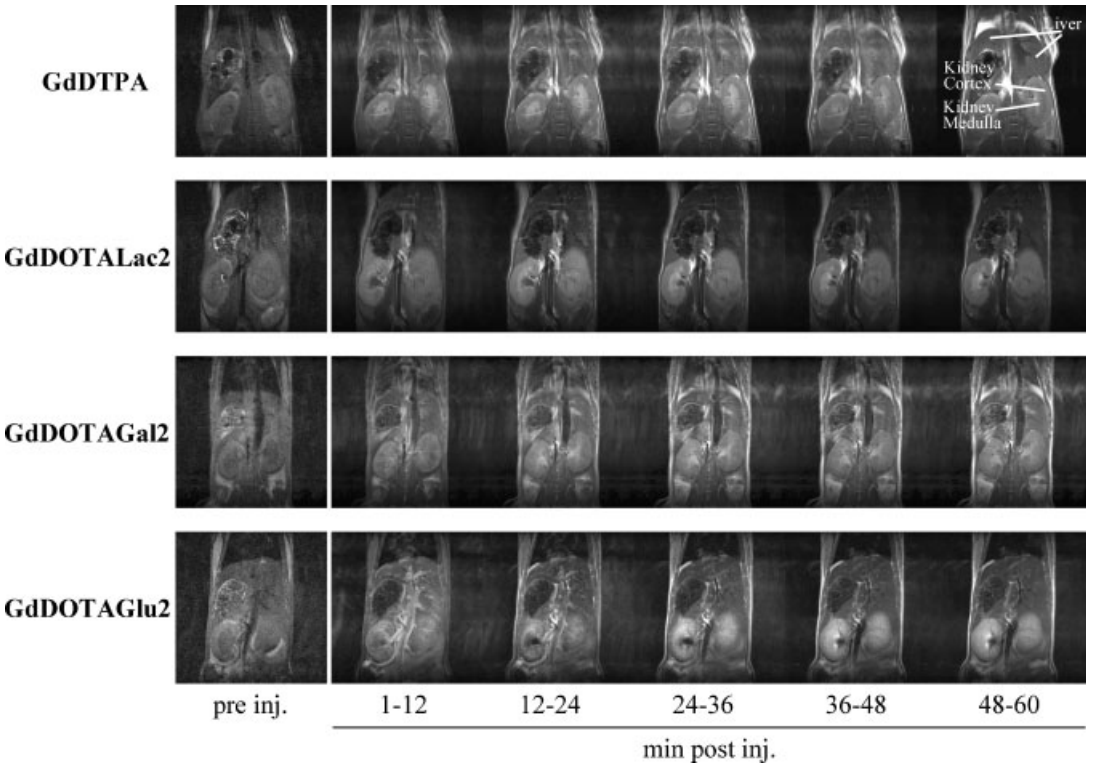

Figure 7. Axial T_1-weighted spin echo MR images of mice before and after injection of GdDTPA (dose 0.2 mmol kg^{-1} BW), $GdDOTALac_2$, $GdDOTAGal_2$ and $GdDOTAGlc_2$ (dose 0.3 mmol kg^{-1} BW). Each image corresponds to the average of 12 min acquisition.

qualitative agreement with that obtained for the interaction with the Hep G2 cell line, although one should consider that the total number of ASGP-R receptors in the human hepatocyte carcinoma cell line HepG2 is $140\,000 \pm 65\,000$ sites per cell (44), significantly lower than the value obtained for isolated rat hepatocytes (37,38).

A DOTA bisamide glycoconjugate bearing two galactosyl moieties in a *cis* position, $DO2A(cis)Gal_2$ (Fig. 1) was also evaluated. Figure 6 shows that this new topology of the targeting groups does not introduce significant differences in the biodistribution pattern at 1 h, although the liver targeting ability of the DOTA monoamide conjugate seems to be superior.

Magnetic resonance imaging

Effect of the Gd chelates on vital functions. The CAs are well tolerated by the mice. No gross side effects were observed during injection, immediately or after the experiment. The animal temperature remained stable throughout the entire experiment, whereas the respiration rate slightly increased during the first 2–3 min post-injection.

MRI in vivo. Series of T_1-weighted spin echo images of the dynamic contrast-enhanced (DCE) MRI experiments with the three divalent DOTA-glycoconjugate chelates of Gd^{3+}, $GdDOTALac_2$, $GdDOTAGal_2$ and $GdDOTAGlc_2$ (dose 0.3 mmol kg^{-1} BW) and GdDTPA (dose 0.2 mmol kg^{-1} BW) are shown in Fig. 7. Before injection, kidney, liver and muscle did not show any contrast difference, due to the short *TR* (155 ms) used for the acquisition of the T_1-weigthed images. After injection, a strong signal enhancement was observed in the kidneys and vena cava, for the various CAs, as a result of the T_1 shortening. A lesser signal enhancement was observed in liver and muscle for all the CAs. The time courses of the average relative enhancement of several ROIs of the T_1-weighted spin echo MR images are displayed in Fig. 8. The scattering in the curves was caused by animal respiratory motion. The time course of the average relative enhancement after the injection of 0.2 mmol/kg of GdDTPA [Fig. 8(a)] is in good agreement with the literature (45). Relative enhancement increased immediately after injection from 0 up to about 300% in the kidney medulla and about 150% in the kidney cortex, liver and muscle. While the enhancement in the later organs remained constant for about 40 min, the kidney medulla value slowly decreased in that time interval to about 200%. The kidney medulla–liver enhancement ratio decreased from 2.2 at 4 min to 1.5 at 35 min. After injection of $GdDOTALac_2$ [Fig. 8(b)], the relative enhancement increased up to approximately 350% in the kidney medulla, 260% in the kidney cortex, 300% in

DOI: 10.1002/cmmi

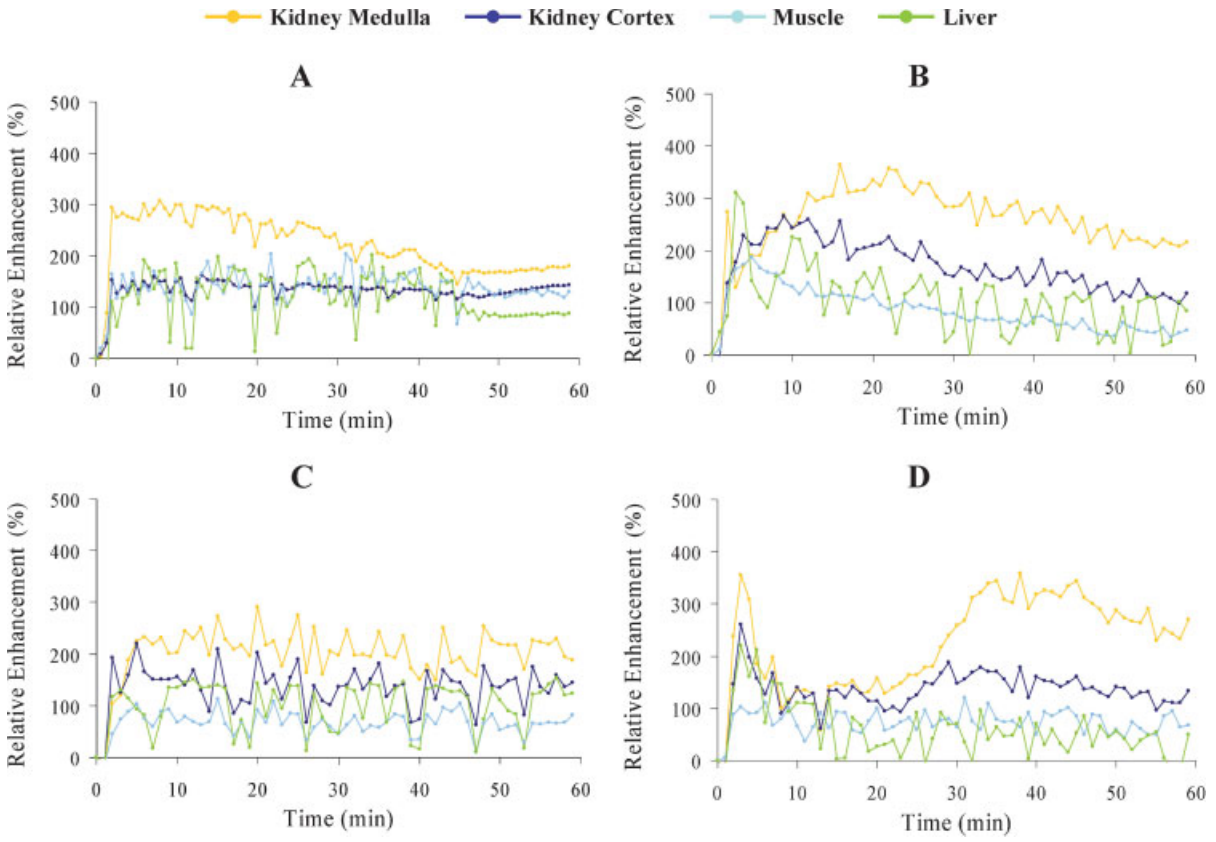

Figure 8. Time course of signal intensity, relative to the initial value (up to 60 min post-injection) of several regions of interest during dynamic contrast enhancement MRI experiments in mice with (A) GdDTPA (dose 0.2 mmol kg^{-1} BW), (B) $GdDOTALac_2$ (dose 0.3 mmol kg^{-1} BW), (C) $GdDOTAGal_2$ (dose 0.3 mmol kg^{-1} BW) and (D) $GdDOTAGlc_2$ (dose 0.3 mmol kg^{-1} BW). The time courses are data for individual animals.

the liver and 180% in the muscle. These maximum enhancements were reached at 20, 10, 3–4 and 4–5 min post-injection, respectively, and then decreased with a slow linear decay. The kidney medulla–liver enhancement ratio increased from 0.6 at 4 min to 4.1 at 35 min. In the case of $GdDOTAGal_2$ [Fig. 8(c)], more moderate increases were observed in all the organs. The relative enhancement increase was approximately 220% in the kidney medulla, 150% in the kidney cortex, 100% in the liver and 80% in the muscle. In all ROIs a plateau was reached within the first 5 min post-injection and remained constant until the end of the pharmacokinetics experiment, with a constant kidney medulla–liver enhancement ratio of 1.7. Finally, immediately after the injection of $GdDOTAGlc_2$ [Fig. 8(d)], a very strong signal rise was observed, especially in the kidney cortex and medulla, followed after 3 min by signal decay due to an effect of T_2 shortening induced by the extremely high concentration of the CA. This circumstance did not allow the maximum enhancement to be measured. Nevertheless, from the measurable points the kidney medulla–liver enhancement ratio increased from 1.6 at 3 min to 5.3 at 35 min.

This comparison of the pharmacokinetics data of the four compounds shows that the glycoconjugate chelates $GdDOTAGlc_2$ and $GdDOTAGal_2$ behave quite similarly to GdDTPA throughout the whole time course of the experiment, with predominant kidney enhancement. In the case of $GdDOTALac_2$ the initial enhancement of liver is higher than of kidney, but after 4 min the kidney cortex and medulla effect becomes predominant.

CONCLUSIONS

Hepatobiliary CAs, with selective hepatocyte uptake by organic anion carriers and biliary excretion, provide a means of obtaining specific liver MRI enhancement and improved detection and characterization of small hepatic lesions (46). Several potential CAs for liver MRI have also been developed by targeting the hepatocyte ASGP-R and uptake via its endocytic pathway, such as targeted particulate T_2 relaxation agents (23–27) and macromolecular T_1 relaxation agents (21,22). This approach is also useful in the detection and characterization of hepatic lesions, as they strongly affect the hepatocyte receptor levels (21). Appending a small glycodendrimer ending with galactosyl unit(s) to a GdDOTA scaffold via an amide bond generates a new class of low molecular weight, stable, hydrophilic glycoconjugates, of greater biological safety than the polymeric GdDTPA-gal-PL (21), and

DOI: 10.1002/cmmi

with targeting ability for the liver via recognition of the ASGP-R, as suggested *in vitro* by Hep G2 cell uptake, and *in vivo* γ-imaging and biodistribution studies of the $[^{153}Sm]^{3+}$-labeled compounds in Wistar rats. The glycodendrimer architecture allows variation of the sugar type and valence in an interactive way from a reduced number of building blocks. The effect of the increase of valence on the targeting efficiency is clear when going from monoderivatives to divalent glycoconjugates. The performance of the next generation, tetravalent glycoconjugates, is similar to that of the divalent one, at 1 h post-injection. However this compound is retained much longer at its target organ, as demonstrated by the activity remaining in the liver after 24 h. Moreover, there are important biodistribution differences between mono- and multivalent glycoconjugates (32). A critical feature in the glycoconjugate–ASGP-R interaction is the topology of both the glycoconjugate and lectin. In this respect, the relative orientation and spacing of the carbohydrate residues in the glycoconjugate in relation to the distribution of the carbohydrate recognition domains (CRDs) on the ASGP-R is of fundamental importance in the optimization of their interaction (47,48).

The superior performance of the multivalent compounds validates our approach to lectin-mediated targeting for molecular imaging. The specific uptake of the galactosyl-bearing compounds via the ASGP-R opened an opportunity for the use of their Gd^{3+} chelates as CAs for ASGP-R mediated liver MRI. However, despite the promising scintigraphic performance of the galactosyl-bearing multivalent compounds, the animal MRI assessment of the corresponding Gd^{3+} chelates shows only limited liver-to-kidney contrast effects, similar to the GdDTPA effects. This probably results from the quick wash-out from the liver to the kidney of these highly hydrophilic complexes, before they can be concentrated within the hepatocytes via receptor-mediated endocytosis up to a concentration high enough to yield a detectable image contrast (49), limiting their use as CAs for ASGP-R-mediated molecular imaging. The design of more efficient hepatocyte-target MRI agents of this kind may be pursued by tuning the hydrophilicity/hydrophobicity balance of the dendrimeric compounds, through either structural modification of the dendrimeric backbone or the sugar-linker moiety, while improving the targeting ability of the multivalent architecture, and enhancing their relaxivity by centrally positioning the Gd^{3+} to provide a more effective motional coupling of the chelate with the Gd^{3+}-proton vector (50).

Acknowledgements

This work was financially supported by the Foundation of Science and Technology (FCT), Portugal (project POCTI/QUI/47005/2002) and FEDER. M.L.G.M. acknowledges financial support from the Institute of Health Carlos III, Spain and T.B.R. an FCT grant (SFRH/BD/5407/2001). The work was carried out within the EC COST Action D18 'Lanthanide chemistry for diagnosis and therapy', the European-funded EMIL programme (LSCH-2004-503569) and the Acção Integrada Luso-Espanhola E-10/04.

REFERENCES

1. Lis H, Sharon N. Lectins: carbohydrate-specific proteins that mediate cellular recognition. *Chem. Rev.* 1998; **98**: 637–674.
2. Gabius H-J, André S, Kaltner H, Siebert H-C. The sugar code: functional lectinomics. *Biochim. Biophys. Acta* 2002; **1572**: 165–177.
3. Dam TK, Brewer CF. Thermodynamic studies of lectin-carbohydrate interactions by isothermal titration calorimetry. *Chem. Rev.* 2002; **102**: 387–429.
4. Loris R. Principles of structures of animal and plant lectins. *Biochim. Biophys. Acta* 2002; **1572**: 198–208.
5. Sharon N, Lis H. *Lectins*, 2nd edn. Kluwer Academic: Dordrecht, 2003.
6. Yamazaki N, Kojima S, Bovin NV, André S, Gabius S, Gabius H-J. Endogenous lectins as targets for drug delivery. *Adv. Drug Deliv. Rev.* 2000; **43**: 225–244.
7. Mammen M, Choi S-K, Whitesides GM. Polyvalent interactions in biological systems: implications for design and use of multivalent ligands and inhibitors. *Angew. Chem. Int. Edn* 1998; **37**: 2754–2794.
8. Lundquist JJ, Toone EJ. The cluster glycoside effect. *Chem. Rev.* 2002; **102**: 555–578.
9. Weigel PH, Yik JHN. Glycans as endocytosis signals: the cases of the asialoglycoprotein and hyaluronan/chondroitin sulfate receptors. *Biochim. Biophys. Acta (General Subjects)* 2002; **1572**: 341–363.
10. Gregoriadis G. Targeting of drugs: implications in medicine. *Lancet* 1981; **2**: 241–246.
11. Deal KA, Criste ME, Welsh MJ. Cellular distribution of ^{111}In-DTPA galactose BSA in normal and asialoglycoprotein receptor-deficient mouse liver. *Nucl. Med. Biol*. 1998; **25**: 379–385.
12. Ishibashi S, Hammer RE, Herz J. Asialoglycoprotein receptor deficiency in mice lacking the minor receptor subunit. *J. Biol. Chem*. 1994; **269**: 27803–27806.
13. Koyama Y, Ishikawa M, Yeda A, Sudo R, Kojima S, Sugunaka A. Body distribution of galactose-containing synthetic-polymer and galactosylated albumin. *Polymer J*. 1993; **25**: 355–361.
14. Vera DR, Stadalnik R, Krohn K. Technetium-99m galactosyl-neoglycoalbumin: preparation and preclinical studies *J. Nucl. Med*. 1985; **10**: 1157–1167.
15. Nakagima K, Kinuya K, Mizutani Y, Hwang EH, Michigishi T, Tonami N, Kobayashi K. Simple scintigraphic parameters with Tc-99m galactosyl human serum albumin for clinical staging of chronic hepatocellular disfunction. *Ann. Nucl. Med*. 1999; **13**: 5–11.
16. Miki K, Kubota K, Inoue Y, Vera DR, Makuuchi M. Receptor measurements via Tc-GSA kinetic modeling are proportional to functional hepatocellular mass *J. Nucl. Med*. 2001; **42**: 733–737.
17. Colquhoum SD, Conelly CA, Vera DR. Portal–systemic shunts reduce asialoglycoprotein receptor density in rats. *J. Nucl. Med*. 2001; **42**: 110–116.
18. Sueyoshi K, Narabayashi I, Aratani T, Doi K, Komori T, Ogura Y, Utsunomiya K, Shimidzu T. Utility of Tc-99m GSA whole-body scintigraphy in detecting bone metastases from hepatocellular carcinoma. *Clin. Nucl. Med*. 2001; **26**: 221–224.
19. Miki K, Kubota K, Kokudo N, Inoue Y, Bandai Y, Makuuchi M. Asialoglycoprotein receptor and hepatic blood flow using technetium-99m-DTPA-galactosyl human serum albumin. *J. Nucl. Med*. 1977; **38**: 1798–1807.
20. Shuke N, Okizaki A, Kino S, Sato J, Ishikawa Y, Zhao CL, Kineya S, Watabane N, Yokoama K, Aburano T. Functional mapping of

regional liver asialoglycoprotein receptor amount from single blood sample and SPECT. *J. Nucl. Med*. 2003; **44**: 475–482.
21. Vera DR, Buonocore MH, Wisner ER, Katzberg RW, Stadalnik RC. A molecular receptor-binding contrast agent for magnetic resonance imaging of the liver. *Acad. Radiol*. 1995; **2**: 497–506.
22. Gallez B, Lacour V, Demeure R, Debuyst R, Dejehet F, Dekeyser JL, Dumont P. Spin labeled arabinogalactan as MRI contrast agent. *Magn. Reson. Imag*. 1994; **12**: 61–69.
23. Schaffer BK, Linker C, Papisov M, Tsai E, Nossiff N, Shibata T, Bogdanov A Jr., Brady TJ, Weissleder R. Mion-ASF: biokinetics of an MR receptor agent. *Magn. Reson. Imag*. 1993; **11**: 411–417.
24. Weissleder R, Reimer P, Lee AS, Wittenberg J, Brady TJ. MR receptor imaging: ultra small iron oxide particles targeted to asialoglycoprotein receptors. *Am. J. Roentgenol*. 1990; **155**: 1161–1167.
25. Reimer P, Weissleder R, Lee AS, Buettner S, Wittenberg J, Brady TJ. Asialoglycoprotein receptor function in benign liver disease: evaluation with MR imaging. *Radiology* 1991; **178**: 769–774.
26. Reimer P, Weissleder R, Wittenberg J, Brady TJ. Receptor-directed contrast agents for MR imaging: preclinical evaluation with afinity assays. *Radiology* 1992; **182**: 565–569.
27. Reimer P, Kwong KK, Weisskoff R, Cohen MS, Brady TJ, Weissleder R. Dynamic signal intensity changes in liver with superparamagnetic MR contrast agents. *J. Magn. Reson. Imag*. 1992; **2**: 177–181.
28. Connoly DT, Townsend RR, Kawagushi K, Bell WR, Lee YC. Binding and endocytosis of cluster glycosides by rabbit hepatocytes. *J. Biol. Chem*. 1982; **257**: 939–945.
29. André JP, Geraldes CFGC, Martins JA, Merbach AE, Prata MIM, Santos AC, de Lima JJP, Tóth E. Lanthanide(III) complexes of DOTA–glycoconjugates: a potential new class of lectin-mediated medical imaging agents. *Chem. Eur. J*. 2004; **10**: 5804–5816.
30. Ḅaía P, André JP, Geraldes CFGC, Martins JA, Merbach AE, Tóth É. Lanthanide(III) complexes of DTPA-bisamide glycoconjugates: potential imaging agents targeted for the asyaloglycoprotein receptor. *Eur. J. lnorg. Chem*. 2005; 2110–2119.
31. Torres S, Martins JA, André JP, Neves M, Santos AC, Prata MIM, Geraldes CFGC. Radiolabelled Sm-153 chelates of glycoconjugates: multivalence and topology effects on the targeting of the asialoglycoprotein receptor. *Radiochimica Acta*, submitted.
32. Alauddin MM, Louie AY, Shahinian A, Meade TJ, Conti PS. Receptor mediated uptake of a radiolabeled contrast agent sensitive to β-galactosidase activity. *Nucl. Med. Biol*. 2003; **30**: 261–265.
33. Brücher E, Sherry AD. Stability and toxicity of contrast agents. In *The Chemistry of Contrast Agents in Medical Magnetic Resonance Imaging*, Merbach AE, Tóth É (eds). Wiley: Chichester, 2001; 243–279.
34. Theilman L, Teicher L, Schildkraut CS, Stockert RJ. Growth-dependent expression of a cell surface glycoprotein. *Biochim. Biophys. Acta* 1983; **762**: 475–477.
35. Hennig J, Nauerth A, Friedburg H. RARE imaging: a fast imaging method for clinical MR. *Magn. Reson. Med*. 1986; **3**: 823–833.
36. Collins JC, Paietta E, Green R, Morell AG, Stockert RJ. Biotin-dependent expression of the asialoglycoprotein receptor in ethanol-fed mice. *J. Biol. Chem*. 1988; **263**: 11280–11283.
37. Schwartz AL, Rup D, Lodish HF. Difficulties in the quantification of asialoglycoprotein receptors on the rat hepatocyte. *J. Biol. Chem*. 1980; **255**: 9033–9036.
38. Weigel PH, Oka JA. The large intracellular pool of asialoglycoprotein receptors functions during the endocytosis of asialoglycoproteins by isolated rat hepatocytes. *J. Biol. Chem*. 1983; **258**: 5095–5102.
39. Vaino AR, Depew WT, Szarek WA. Synthesis of a D-lactosyl cluster–nucleoside conjugate. *Chem. Commun*. 1997; 1871–1872.
40. Krebs A, Depew WT, Szarek WA, Hay GW, Hronowski LJJ. Binding of D-galactose-terminated ligands to rabbit asialoglycoprotein receptor. *Carbohydr. Res*. 1994; **254**: 257–268.
41. Lee YC, Townsend RR, Hardy MR, Lönngren J, Arnarp J, Haraldsson M, Lönn H. Binding of synthetic oligosaccharides to the hepatic Gal/GalNAc lectin. Dependence on fine structural features. *J. Biol. Chem*. 1983; **258**: 199–202.
42. Lee RT, Lee YC. Rabbit and rat hepatic lectins have two sugar-combining sites per monomeric unit. *Biochem. Biophys. Res. Commun*. 1988; **155**: 1444–1451.
43. Biessen EAL, Broxterman H, VanBoom JH, VanBerkel TJ. The cholesterol derivative of a triantennary galactoside with high affinity for the hepatic asialoglycoprotein receptor: a potent cholesterol lowering agent. *J. Med. Chem*. 1995; **38**: 1846–1852.
44. Eisenberg C, Seta N, Appel M, Feldmann G, Durand G, Feger J. Asialoglycoprotein receptor in human isolated hepatocytes from normal liver and its apparent increase in liver with histological alterations. *J Hepatol*. 1991; **13**: 305–309.
45. Raghunand N, Howison C, Sherry AD, Zhang S, Gillies RJ. Renal and systemic pH imaging by contrast-enhanced MRI. *Magn. Reson. Med*. 2003; **49**: 249–257.
46. Van Beers BE, Gallez B, Prigot J. Contrast-enhanced MR imaging of the liver. *Radiology* 1997; **203**: 297–306.
47. Vrasidas I, André S, Valentini P, Bock C, Lensch M, Kaltner H, Liskamp RMJ, Gabius H-J, Pieters RJ. Rigidified multivalent lactose molecules and their interactions with mammalian galectins: a route to selective inhibitors. *Org. Biomol. Chem*. 2003; **1**: 803–810.
48. Meier M, Bider MD, Malashkevich VN, Spiess M, Burkhard P. Crystal structure of the carbohydrate recognition domain of the H1 subunit of the asialoglycoprotein receptor. *J. Mol. Biol*. 2000; **300**: 857–865.
49. Aime S, Barge A, Cabella C, Geninatti Crich S, Gianolio E. Targeting cells with MR imaging probes based on paramagnetic Gd(III) chelates. *Curr. Pharm. Biotechnol*. 2004; **5**: 509–518.
50. Fulton DA, Elemento EM, Aime S, Chaabane L, Botta M, Parker D. Glycoconjugates of gadolinium complexes for MRI applications. *Chem. Commun*. 2006; 1064–1066.

DOI: 10.1002/cmmi